Dynamic Self-Organization of Idealized Migrating Cells by Contact Communication

Tetsuya Hiraiwa*
Mechanobiology Institute, National University of Singapore, 117411, Singapore and Universal Biology Institute, The University of Tokyo, Hongo, Tokyo 113-0033, Japan

(Received 2 July 2020; accepted 4 December 2020; published 31 December 2020)

This Letter investigates what forms of cellular dynamic self-organization are caused through intercellular contact communication based on a theoretical model in which migrating cells perform contact following and contact inhibition and attraction of locomotion. Tuning those strengths causes varieties of dynamic patterns. This further includes a novel form of collective migration, snakelike dynamic assembly. Scrutinizing this pattern reveals that cells in this state can accurately respond to an external directional cue but have no spontaneous global polar order.

DOI: 10.1103/PhysRevLett.125.268104

The emergence of dynamics can be a versatile concept to understand how living systems acquire complex structures and functions. Cells, the fundamental elements of living systems, often move cooperatively and spontaneously organize their dynamic patterns. Such dynamic self-organization (DSO) is accompanied by cooperative movement of cells through intercellular communication, as revealed for neural crest cells in *Xenopus* and chicken embryos [1–6] and the cellular slime mold *Dictyostelium discoideum* (Dicty) [7–12], and can influence functional biological processes. For example, collective cell migration is relevant for cells to respond accurately to environmental factors, perform mechanically efficient dynamics, and achieve proper morphogenesis in multicellular organisms [4–6,13–18]. In light of this, various theoretical models have been proposed based on different frameworks to simulate cooperative migration and investigate their mechanisms and functional roles [19], e.g., agent-based [6,20–22], semimechanistic [23,24], phase field [25], cellular Potts [26], and vertex and Voronoi tessellation [27–29] frameworks.

Over the past decade, biologists have accumulated knowledge on the nature and role of contact communication between migrating cells, such as so-called contact following (CF) and contact inhibition and attraction of locomotion (CIL and CAL, respectively). In CF, when a cell contacts another cell, the cell at the back chases the cell at the front but not vice versa [Fig. 1(a)]. CF has been observed in several cells [9,12,30] and revealed to be involved in various types of DSO [9,12]. In CIL, when two cells come in contact, they exchange information and modulate their polarities to avoid overlap [Fig. 1(b)] [2,5,6,13,14]. For instance, *Xenopus* neural crest cells undergoing CIL are seen to scatter [2]. CIL is involved in coordinated migration and directional migration in response to external cues [5,6]. On the other hand, in CAL, contacting cells are mutually attracted [Fig. 1(b)], which may contribute to their coordinated behaviors [3]. Thus, contact-mediated mechanisms can play versatile roles in cellular DSO. However, there is a lack of a unified model capable of achieving various types of cellular DSO only through contact communication. To thoroughly investigate the mechanisms underlying cellular DSO and its potential biological functions, such a model is indispensable.

In this Letter, I propose a theoretical model of cells migrating on a substrate in two dimensions which generates a variety of DSO patterns solely through cellular contact interactions, based on the framework for collective motion of polar self-propelled elements. These elements move around according to their intrinsic polarity by consumption of input energy [31]. Their collective motion has been intensively investigated over the past decades, which has revealed that interaction between motile elements are significant factors to control collective behaviors [31–48]. Here, cells are ideally regarded as self-propelled disk-shaped particles with volume exclusion (VE), and local

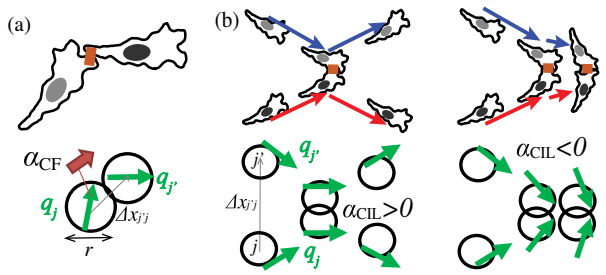

FIG. 1. Schematics of the types of intercellular communication in the model. (a) Contact following. The strength is denoted by α_{CF}. (b) Contact inhibition and attraction of locomotion (left and right, respectively). The strength is denoted by α_{CIL}. In each, the top and bottom subfigures describe the cases for cell migration and idealized situations, respectively. Green arrows indicate intrinsic polarities of cells, $\boldsymbol{q}_j$ (for the jth cell).

 © 2020 American Physical Society

pairs of particles modulate their intrinsic polarities through contact interactions. The major focus of this Letter is to highlight the significance of contact communication in achieving a myriad of DSO patterns.

We approximate each migrating cell as a self-propelled particle in two dimensions [49,50]. We model N cells by the equation of motion

$$\frac{d\boldsymbol{x}_j}{dt} = v_0 \boldsymbol{q}_j + \boldsymbol{J}^v{}_j \tag{1}$$

and polarity angle dynamics

$$\frac{d\theta_j}{dt} = \boldsymbol{J}^q{}_j \cdot \boldsymbol{q}_{j,\perp} + \boldsymbol{f}_j \cdot \boldsymbol{q}_{j,\perp} + \xi_j \tag{2}$$

of each jth cell ($j = 1, 2, \ldots, N$) with its center position $x_j(t)$ at time t, intrinsic polarity $\boldsymbol{q}_j(t) \equiv [\cos\theta_j(t), \sin\theta_j(t)]$, and $\boldsymbol{q}_{j,\perp} = (-\sin\theta_j, \cos\theta_j)$. Equation (1) assumes overdamped dynamics, and v_0 is the spontaneous migration speed. Assuming each cell as a soft disk with fixed radius r, VE is given by $\boldsymbol{J}^v{}_j = -\beta \sum_{j'(n.j)} (r|\Delta\boldsymbol{x}_{j'j}|^{-1} - 1)\widehat{\Delta\boldsymbol{x}_{j'j}}$, where $\Delta\boldsymbol{x}_{j'j} = \boldsymbol{x}_{j'} - \boldsymbol{x}_j$ and $\widehat{\Delta\boldsymbol{x}_{j'j}} = \Delta\boldsymbol{x}_{j'j}/|\Delta\boldsymbol{x}_{j'j}|$ and the summation $\sum_{j'(n.j)}$ runs for all neighbors of the jth cell defined by $|\Delta\boldsymbol{x}_{j'j}| < r$ (Fig. S1 in Supplemental Material [51]). $\boldsymbol{J}^q{}_j$ represents intercellular communication. $\xi_j(t)$ is a white Gaussian noise satisfying $\langle\xi_j\rangle = 0$ and $\langle\xi_i(t)\xi_j(t')\rangle = 2D\delta_{ij}\delta(t-t')$, and D is the noise dispersion. We apply external directional bias $\boldsymbol{f}_j$ at the end, where we set a constant vector $\boldsymbol{f}_j = (0, A)$ among all cells. (See Supplemental Material for more model details [51].) This model is highly idealized, but still the models based on the same framework captured several features of cell migration [12,22,49].

In this Letter, $\boldsymbol{J}^q{}_j$ consists of CF and CIL as $\boldsymbol{J}^q{}_j = \boldsymbol{J}^{\mathrm{CF}}{}_j + \boldsymbol{J}^{\mathrm{CIL}}{}_j$, where

$$\boldsymbol{J}^{\mathrm{CF}}{}_j = \alpha_{\mathrm{CF}} \sum_{j'(n.j)} \frac{1 + \widehat{\Delta\boldsymbol{x}_{j'j}} \cdot \widehat{\boldsymbol{q}_{j'}}}{2} \widehat{\Delta\boldsymbol{x}_{j'j}} \tag{3}$$

and

$$\boldsymbol{J}^{\mathrm{CIL}}{}_j = -\alpha_{\mathrm{CIL}} \sum_{j'(n.j)} (r|\Delta\boldsymbol{x}_{j'j}|^{-1} - 1)\widehat{\Delta\boldsymbol{x}_{j'j}} \tag{4}$$

(Fig. S1 [51]) with the strengths α_{CF} (≥ 0) and α_{CIL} (> 0 for CIL; < 0 for CAL; $= 0$ otherwise), respectively. To get initial insights, the interaction terms presented here are compared with those discussed in earlier literature. CF is a nonreciprocal local interaction with forward-backward asymmetry [Fig. 1(a)], similar to the chasing interaction assumed in the escape-and-pursuit and cognitive flocking models [35,39,47]. CIL can be regarded as a short-range repulsion acting on the intrinsic polarity $\boldsymbol{q}$ [Fig. 1(b)], which is similar to local cognitive repulsion in the animal group model [35]. CIL combined with VE can lead to pair behavior of self-propelled particles analogous to inelastic collision, which effectively causes alignment [22,54–56]. Here, CAL is treated simply as the negative direction of CIL [Fig. 1(b)] and can be regarded as a short-range attraction on $\boldsymbol{q}$. Referring to earlier work by Grossmann, Schimansky-Geier, and Romanczuk [44], which investigated the consequences of short-range selective attraction and repulsion, the model presented here is also expected to exhibit polar traveling bands and homogeneous polar flocking for $\alpha_{\mathrm{CIL}} > 0$ (repulsion) whereas aggregation for $\alpha_{\mathrm{CIL}} < 0$ (attraction).

We numerically simulate Eqs. (1)–(4) in a 2D regular square with area W and the periodic boundary condition. We formulate dimensionless equations using characteristic length $X \equiv r$ and time $T \equiv r/v_0$ [22]. For this, we can simply put $r = 1$ and $v_0 = 1$. We apply the Heun's method with the increment time step $dt = 0.01$ up to $t = 6400$ unless mentioned specifically. The total number of cells N is given for each simulation, and $W = N/\rho$. Throughout this Letter, we use $D = 0.1$, which is comparable with a single-cell migration data [49,51]. $1/D$ corresponds to the persistence time of the migrating direction of a solitary cell [49]. For simplicity, we set $\rho = 1.0$ and $\beta = 1.0$. (The case for $\beta = 0$ is discussed in Supplemental Material [51].) Note that, with these values of D and ρ, motility-induced phase separation [42,43] does not occur and a homogeneous disorder state is observed for $\alpha_{\mathrm{CF}} = \alpha_{\mathrm{CIL}} = 0$ [22].

By varying α_{CF} and α_{CIL}, this model undergoes various DSO patterns as shown in Fig. 2(a) for $A = 0.0$ and $N = 10000$. Figures 2(b)–2(d) show the patterns observed in the absence of CIL ($\alpha_{\mathrm{CIL}} = 0.0$). When $\alpha_{\mathrm{CF}} > 0.8$, cells form rings [Fig. 2(b) and Supplemental Material [51]] similarly to Refs. [35,47]. For smaller α_{CF} as $0.8 \geq \alpha_{\mathrm{CF}} \geq 0.5$, ring formation fails [Fig. 2(c)]. For even smaller α_{CF}, $0.5 \geq \alpha_{\mathrm{CF}} > 0.3$, we find dynamic assemblies with thick snakelike shapes, which keep repeating to gather and scatter [Fig. 2(d) and Movie S1 [51]]. We call this pattern snakelike dynamic assembly (SDA). All these patterns are made of stripe-shaped clusters, which may be regarded as the analogy for the presence of VE of the wormlike pattern in a cognitive flocking model [47]. In the stripe, cell polarities are directed nearly toward the stripe's center line but spontaneously tilted to either direction parallel to the stripe so that the cluster moves in that direction [Fig. 2(e)].

For $\alpha_{\mathrm{CIL}} > 0.0$, polarly ordered patterns appear. CF decreases the threshold α_{CIL} to form the traveling band [Fig. 2(f)]. Similar CF-assisted traveling band formation was investigated in our previous work for the model with a different cell-cell interaction [12]. Larger α_{CIL} turns traveling bands into the homogeneous order [Fig. 2(g)]. These

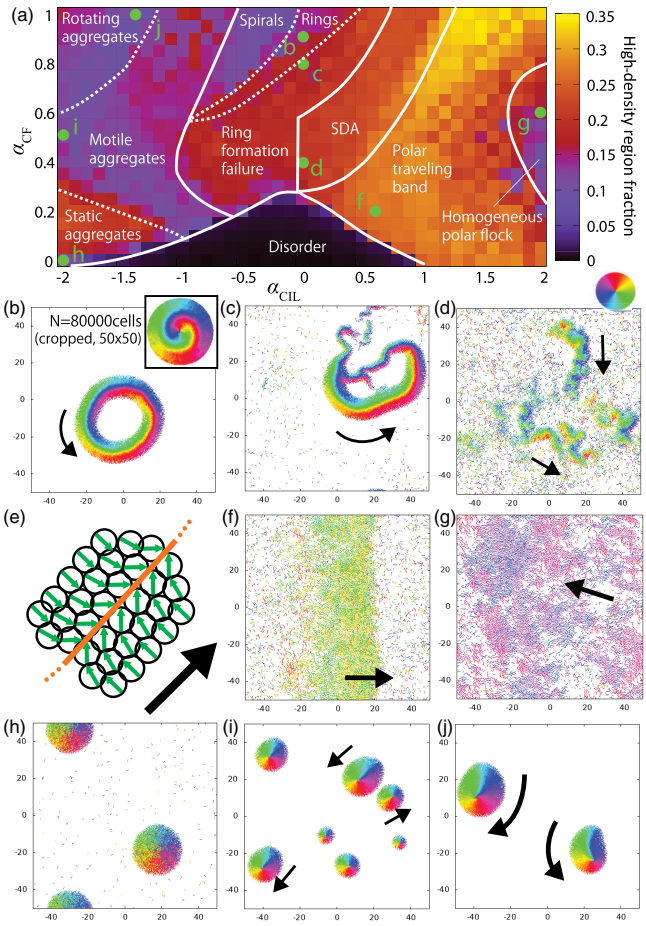

FIG. 2. Phase diagram for $\beta = 1.0$, $D = 0.1$, $A = 0.0$, $\rho = 1.0$, and $N = 10000$. (a) Fraction of space covered by high-density regions [51], against α_{CF} and α_{CIL}. (See Fig. S2 for the heat maps of other quantities [51].) Curves indicate the phase boundaries [51]. Broken curves specifically indicate the apparent phase boundaries expected to disappear for the large N and long-time limits. (b)–(d),(f)–(j) Snapshots. Each small colored arrow represents the location and polarity direction of each cell, and the color indicates the polarity direction corresponding to the color wheel for better visibility. Large black arrows indicate the apparent motile directions of clusters. The observed patterns include (b) ring and spiral, (c) ring-formation failure, (d) SDA, (f) polar traveling band, (g) homogeneous polar flock, (h) static aggregate, (i) motile aggregate, and (j) rotating aggregate. The values of α_{CF} and α_{CIL} for each snapshot are indicated in (a) by the marks. Figure S3 displays more snapshots [51]. (e) Schematic showing directions of each cell polarity and stripe-shaped cluster's motion (green and large black arrows, respectively) in (b)–(d). Orange line describes the stripe's center line.

traveling bands may emerge through microphase separation like the Vicsek model [57]. Indeed, multiple bands are observed for $N = 80000$ (Fig. S4 [51]).

CAL ($\alpha_{CIL} < 0.0$) induces aggregation patterns as I reported previously [22] [Fig. 2(h) and Movie S2 [51]]. When we further add CF for $\alpha_{CIL} < 0.0$, aggregations become motile and fluctuating [Fig. 2(i) and Movie S3 [51]]. With further higher α_{CF}, the motile trajectory of an aggregation draws rotation [Fig. 2(j) and Movie S4 [51]]. This set of bifurcations resembles those of a single deformable self-propelled particle [40,58,59].

Here, N dependency is briefly clarified, since it is generally well recognized in collective motion [36,38,60]. For the larger system $N = 80000$, spirals coexist with stable rings. Some spirals were apparently stable during the simulation time [Fig. 2(b), inset] (a similar pattern was also obtained by the pursuit model [39]), while the others intermittently move. See Movie S5 [51], in which all these patterns coexist in a single simulation. Also, ring-formation failure in Fig. 2(c) was not observed for $\alpha_{CF} = 0.6$, 0.7, 0.8 and $\alpha_{CIL} = 0$ with $N = 80000$. Collectively, the distinction between these apparent three phases may stem from the finite N effect. Furthermore, three different dynamics of aggregates in Figs. 2(h)–2(j) can depend on the cell number in each aggregate as well as parameter values (Supplemental Material [51]).

Among these varieties, SDA is a novel DSO pattern. We now scrutinize its nature with larger N, up to 80000 [Fig. 3(a) and Movies S7 and S8 [51]]. The mechanism generating SDA can be understood by the competition between CF and CIL: While CIL may enhance the diffusion perpendicular to the traveling direction of surrounding local cell population, CF may hinder it, which prevents band formation and leads to SDA. Indeed, this mechanism is reflected in Fig. 3(b) with the mean square displacement in the transverse direction, $\mathrm{tMSD}(\Delta t) \equiv \overline{|\int_0^{\Delta t} dt' \hat{\boldsymbol{V}}_{n.j}(t_0 + t') \times \boldsymbol{v}_j(t_0 + t')|^2}$ with a lag time Δt. Here, $\hat{\boldsymbol{V}}_{n.j}(t)$ is the unit vector along the average migration direction of neighbors (cells within the distance r) around the jth cell, $\times$ is the cross product, and the average $\bar{\cdot}$ runs for cells j locating in the dense region (defined such that the cell number density within the distance r around the jth cell is > 1.50) and time t_0. For large α_{CIL} yielding traveling bands, $\mathrm{tMSD} \propto (\Delta t)^1$ between $\Delta t \sim 10$ and several hundred like the normal diffusion. When α_{CF} is decreased and exceeds the transition threshold to SDA, $\mathrm{tMSD}(\Delta t)$ exhibits subdiffusive behavior for this intermediate Δt.

To investigate whether SDA has global polar order (PO), we measured the PO parameter $R = |\sum_{j=1}^{N} \boldsymbol{q}_j / N|$ [Fig. 3(c)]. R within the SDA state ($0.28 \leq \alpha_{CF} \leq 0.56$ for $\alpha_{CIL} = 0.0$) decreases for increasing N [Fig. 3(d)], suggesting that R can vanish in the large N limit. To further confirm this, we measured dependency of the local PO R_l on the size l of each region of interest (ROI). Indeed, R_l decreases, even though it can be quite slow, for increasing l [Fig. 3(e) and the inset]. Altogether, this SDA state is qualitatively distinct from the other states including disorder and traveling band states.

Finally, to seek possible functional relevance of various DSO patterns, we ask how they influence collective directional migration, e.g., due to external gradients (chemotaxis).

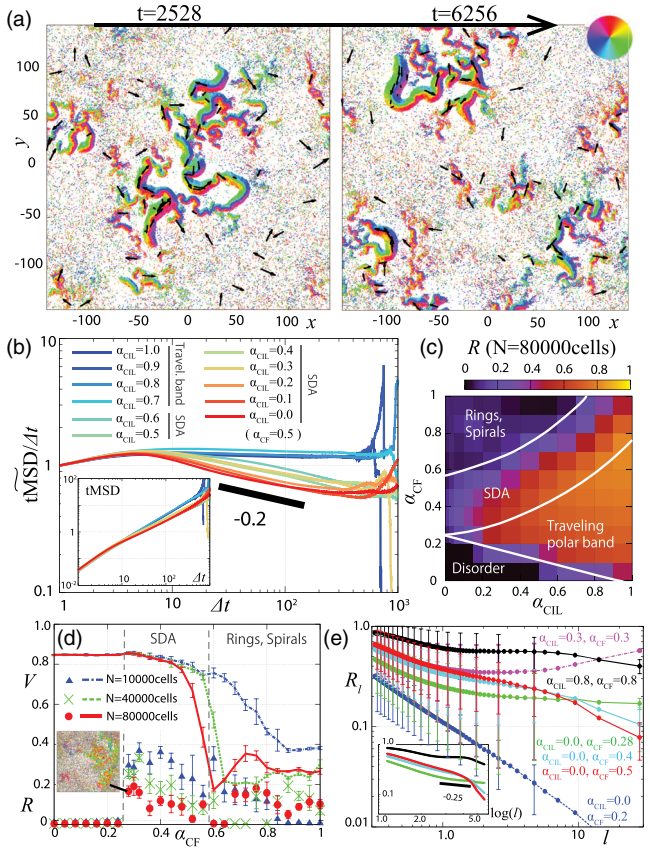

FIG. 3. SDA, for $\beta = 1.0$, $D = 0.1$, and $\rho = 1.0$. $N = 80000$ except for (d). (a) Snapshots for $\alpha_{\mathrm{CF}} = 0.5$ and $\alpha_{\mathrm{CIL}} = 0.0$. Small colored arrows are defined in the Fig. 2 legend. Black arrows indicate the velocity vectors of 80 representative cells. See also Movie S7 [51]. (b) tMSD(Δt) for $\alpha_{\mathrm{CF}} = 0.5$ and various α_{CIL}. Main: $\widetilde{\mathrm{tMSD}} \equiv \mathrm{tMSD}(\Delta t)/\mathrm{tMSD}(1)$ divided by Δt. Inset: tMSD itself. For (b), simulations were performed up to $t = 9600$. (c) Global PO R against α_{CIL} and α_{CF}. Figure S4 displays the corresponding snapshots [51]. (d) R (marks) and median cell speed V (curves) for $\alpha_{\mathrm{CIL}} = 0.0$ for various α_{CF} and N. (e) ROI linear size l dependence of local PO R_l (i.e., PO parameter calculated in rectangular ROIs with size $l \times l$). Inset: $\log(l)$ dependence of R_l for the SDA state. Thick line segments are eye guides for power-law slopes. Error bars indicate standard deviations over time for (d) and time and ROIs for (e).

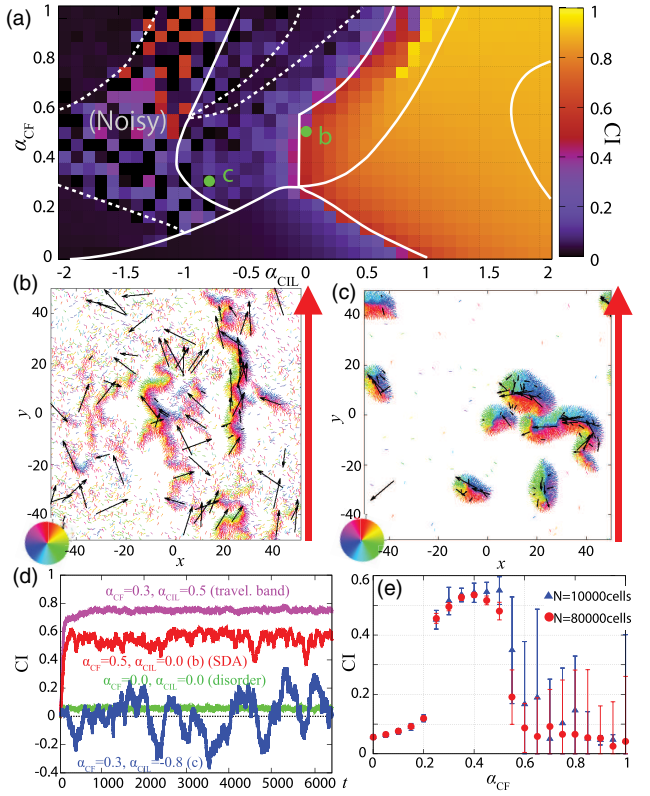

FIG. 4. Directional migration under external directional bias $A = 0.01$ for $\beta = 1.0$, $D = 0.1$, and $\rho = 1.0$ with $N = 10000$ for (a)–(d). (a) CI for various α_{CF} and α_{CIL}. Curves indicate the phase boundaries determined for $A = 0.0$ [Fig. 2(a)]. (b),(c) Snapshots. The parameter values are indicated in (a). Small colored and black arrows are defined in the Fig. 2 and 3 legends, respectively. Huge red arrows indicate the bias direction. Figure S5 displays more snapshots [51]. (d) CI calculated in each frame for various α_{CF} and α_{CIL}. (e) CI for $\alpha_{\mathrm{CIL}} = 0.0$ for various α_{CF} and N. Marks and error bars indicate means and standard deviations over time, respectively.

We apply external directional bias $A = 0.01$ and investigate the accuracy of directional responses of cells [Figs. 4(a)–4(c)], by quantifying $\mathrm{CI} \equiv (1/N)\sum_j^N \cos(\theta_j^v)$, called the chemotaxis index (CI), with the angle θ_j^v of the jth cell's motion direction around the bias direction. This A's value is small enough such that, if cells have no cell communications, they hardly respond to the bias (CI < 0.1) [Fig. 4(d), green curve]. Even under such faint bias, cells undergo accurate directional motion in the SDA state, $0.25 \leq \alpha_{\mathrm{CF}} \leq 0.5$ (red curve), like in traveling bands (purple curve) [Figs. 4(a) and 4(d)]. Strikingly, unlike the global PO, CI sustains for larger cell numbers, $N = 80000$ [Fig. 4(e)]. The other states lacking global PO bring no robust improvement of directional accuracy [Figs. 4(a), 4(c), and 4(d), blue curve]. In Fig. 4(c), clusters almost randomly move around much more slowly than solitary cells, and that is why CI largely fluctuates across zero. In contrast, in Fig. 4(b), small SDAs travel accurately toward the bias (Movie S9 [51]). This might be due to weak correlations of motile directions across small SDAs, which is indeed seen even when $A = 0.0$ in Movie S7 [51].

Through the model I proposed in this Letter, I have shown how various DSO patterns are induced through contact interactions of varying strengths, including CF, CIL, and CAL (Figs. 1 and 2). The obtained patterns cover several types of DSO observed in cells. (See Supplemental Material for examples for Dicty cells [51].) However, in living cells, nonlocal communication through secreted chemicals, such as autochemotactic signaling of Dicty cells [7] and neural crest cells [6], also plays some role, which is not incorporated in the presented model. Nevertheless, underestimation of contact-mediated

mechanisms should be avoided when a certain DSO is desired to be explained. The model presented here demonstrates possibilities of contact communications to explain DSO varieties without introducing extra fields or nonlocal mechanisms.

Furthermore, this model can predict what patterns can emerge from contact interaction. As a new finding, I have shown that cells with CF can form SDA, which has polar order locally but no global order (Fig. 3). Even without global order, cells in the SDA state can achieve accurate directional motion toward a faint external cue (Fig. 4). This result proposes a new mechanism of collective migration with high directional accuracy that possibly relies solely on DSO due to paired contact communication, distinct from the mechanisms involving collective sensing and long-range interaction [6,21].

I express my gratitude to T. Ohta and the anonymous reviewers for critical reading of the manuscript and important comments. I thank the MBI science communication core's A. Wong and S. Jagannathan for editing the manuscript. I appreciate the fruitful discussions with T. Shibata and M. Hayakawa from our previous work, which greatly motivated this work. I also thank A. Nakajima, S. Sawai, N. Saito, M. Sano, Y. Nakaya, R. Akiyama, Y. Toyama, and T. B. Saw for valuable comments. This research was supported by Mechanobiology Institute, National University of Singapore, and the JSPS KAKENHI Grants No. JP16K17777 and No. JP19K03764.

*mbithi@nus.edu.sg

[1] R. Mayor and C. Carmona-Fontaine, Keeping in touch with contact inhibition of locomotion, Trends Cell Biol. **20**, 319 (2010).

[2] C. Carmona-Fontaine, H. K. Matthews, S. Kuriyama, M. Moreno, G. A. Dunn, M. Parsons, C. D. Stern, and R. Mayor, Contact inhibition of locomotion in vivo controls neural crest directional migration, Nature (London) **456**, 957 (2008).

[3] Y. Li, F. M. Vieceli, W. G. Gonzalez, A. Li, W. Tang, C. Lois, and M. E. Bronner, In vivo quantitative imaging provides insights into trunk neural crest migration, Cell Rep. **26**, 1489 (2019).

[4] E. Theveneau and R. Mayor, Neural crest delamination and migration: From epithelium-to-mesenchymetransition to collective cell migration, Dev. Biol. **366**, 34 (2012).

[5] E. Theveneau, L. Marchant, S. Kuriyama, M. Gull, B. Moepps, M. Parsons, and R. Mayor, Collective chemotaxis requires contact-dependent cell polarity, Dev. Cell **19**, 39 (2010).

[6] C. Carmona-Fontaine, E. Theveneau, A. Tzekou, M. Tada, M. Woods, K. M. Page, M. Parsons, J. D. Lambrisand, and R. Mayor, Complement fragment C3a controls mutual cell attraction during collective cell migration, Dev. Cell **21**, 1026 (2011).

[7] T. Gregor, K. Fujimori, N. Masaki, and S. Sawai, The onset of collective behavior in social amoebae, Science **328**, 1021 (2010).

[8] K. Müller and G. Gerisch, A specific glycoprotein as the target site of adhesion blocking Fab in aggregating dictyostelium cells, Nature (London) **274**, 445 (1978).

[9] T. Fujimori, A. Nakajima, N. Shimada, and S. Sawai, Tissue self-organization based on collective cell migration by contact activation of locomotion and chemotaxis, Proc. Natl. Acad. Sci. U.S.A. **116**, 4291 (2019).

[10] J. L. Dynes, A. M. Clark, G. Shaulsky, A. Kuspa, W. F. Loomis, and R. A. Firtel, LagC is required for cell-cell interactions that are essential for cell-type differentiation in dictyostelium, Genes Dev. **8**, 948 (1994).

[11] H. Kuwayama and S. Ishida, Biological soliton in multicellular movement, Sci. Rep. **3**, 2272 (2013).

[12] M. Hayakawa, T. Hiraiwa, Y. Wada, H. Kuwayama, and T. Shibata, Polar pattern formation induced by contact following locomotion in a multicellular system, eLife **9**, e53609 (2020).

[13] R. A. Desai, S. B. Gopal, S. Chen, and C. S. Chen, Contact inhibition of locomotion probabilities drive solitary versus collective cell migration, J. R. Soc. Interface **10**, 20130717 (2013).

[14] B. Lin, T. Yin, Y. I. Wu, T. Inoue, and A. Levchenko, Interplay between chemotaxis and contact inhibition of locomotion determines exploratory cell migration, Nat. Commun. **6**, 6619 (2015).

[15] C. P. McCann, P. W. Kriebel, C. A. Parent, and W. Losert, Cell speed, persistence and information transmission during signal relay and collective migration, J. Cell Sci. **123**, 1724 (2010).

[16] D. Cai, W. Dai, M. Prasad, J. Luo, N. S. Gov, and D. J. Montell, Modeling and analysis of collective cell migration in an in vivo three-dimensional environment, Proc. Natl. Acad. Sci. U.S.A. **113**, E2134 (2016).

[17] D. Ellison, A. Mugler, M. D. Brennan, S. H. Lee, R. J. Hueber, E. R. Shamir, L. A. Woo, J. Kim, P. Amar, I. Nemenman, A. J. Ewald, and A. Levchenko, Cell-cell communication enhances the capacity of cell ensembles to sense shallow gradients during morphogenesis, Proc. Natl. Acad. Sci. U.S.A. **113**, E679 (2016).

[18] O. Nagel, M. Frey, M. Gerhandt, and C. Beta, Harnessing motile amoeboid cells as trucks for microtransport and -assembly, Adv. Sci. **6**, 1801242 (2019).

[19] Several review articles are available, e.g., A. Szabó and R. Mayor, Modelling collective cell migration of neural crest, Curr. Opin. Cell Biol. **42**, 22 (2016); B. A. Camley and W.-J. Rappel, Physical models of collective cell motility: From cell to tissue, J. Phys. D **50**, 113002 (2017); V. Hakim and P. Silbersan, Collective cell migration: A physics perspective, Rep. Prog. Phys. **80**, 076601 (2017); R. Alert and X. Trepat, Physical models of collective cell migration, Annu. Rev. Condens. Matter Phys. **11**, 77 (2020).

[20] M. Meyer, L. Schimansky-Geier, and P. Romanczuk, Active Brownian agents with concentration-dependent chemotactic sensitivity, Phys. Rev. E **89**, 022711 (2014).

[21] B. A. Camley, J. Zimmermann, H. Levine, and W.-J. Rappel, Emergent Collective Chemotaxis Without Single-Cell Gradient Sensing, Phys. Rev. Lett. **116**, 098101 (2016).

[22] T. Hiraiwa, Two types of exclusion interactions for self-propelled objects and collective motion induced by their combination, Phys. Rev. E **99**, 012614 (2019).

[23] B. Szabó, G. J. Szöllösi, B. Gönci, Zs. Jurányi, D. Selmeczi, and T. Vicsek, Phase transition in the collective migration of tissue cells: Experiment and model, Phys. Rev. E **74**, 061908 (2006).
[24] S. K. Schneider, J. J. Molina, Y. Tanaka, and R. Yamamoto, Collective motion of cells crawling on a substrate: Roles of cell shape and contact inhibition, Sci. Rep. **7**, 5163 (2017); M. Campo, S. K. Schnyder, J. J. Molina, T. Speck, and R. Yamamoto, Spontaneous spatiotemporal ordering of shape oscillations enhances cell migration, Soft Matter **15**, 4939 (2019).
[25] J. Löber, F. Ziebert, and I. S. Aranson, Collisions of deformable cells lead to collective migration, Sci. Rep. **5**, 9172 (2015).
[26] K. Matsushita, Cell-alignment patterns in the collective migration of cells with polarized adhesion, Phys. Rev. E **95**, 032415 (2017); Emergence of collective propulsion through cell-cell adhesion, Phys. Rev. E **97**, 042413 (2018).
[27] B. Li and S. X. Sun, Coherent motions in confluent cell monolayer sheets, Biophys. J. **107**, 1532 (2014).
[28] D. Bi, X. Yang, M. C. Marchetti, and M. L. Manning, Motility-Driven Glass and Jamming Transitions in Biological Tissues, Phys. Rev. X **6**, 021011 (2016).
[29] D. L. Barton, S. Henkes, C. J. Weijer, and R. Sknepnek, Active vertex model for cell-resolution description of epithelial tissue mechanics, PLoS Comput. Biol. **13**, e1005569 (2017).
[30] D. Li and Y. Wang, Coordination of cell migration mediated by site dependent cell-cell contact, Proc. Natl. Acad. Sci. U.S.A. **115**, 10678 (2018).
[31] T. Vicsek and A. Zafeiris, Collective motion, Phys. Rep. **517**, 71 (2012).
[32] T. Vicsek, A. Czirók, E. Ben-Jacob, I. Cohen, and O. Shochet, Novel Type of Phase Transition in a System of Self-Driven Particles, Phys. Rev. Lett. **75**, 1226 (1995).
[33] N. Shimoyama, K. Sugawara, T. Mizuguchi, Y. Hayakawa, and M. Sano, Collective Motion In a System of Motile Elements, Phys. Rev. Lett. **76**, 3870 (1996).
[34] H. Levine, W.-J. Rappel, and I. Cohen, Self-organization in systems of self-propelled particles, Phys. Rev. E **63**, 017101 (2000).
[35] I. D. Couzin, J. Krause, R. James, G. D. Ruxton, and N. R. Franks, Collective memory and spatial sorting in animal groups, J. Theor. Biol. **218**, 1 (2002).
[36] G. Grégoire and H. Chaté, Onset of Collective and Cohesive Motion, Phys. Rev. Lett. **92**, 025702 (2004).
[37] M. R. D'Orsogna, Y. L. Chuang, A. L. Bertozzi, and L. S. Chayes, Self-Propelled Particles with Soft-Core Interactions: Patterns, Stability, and Collapse, Phys. Rev. Lett. **96**, 104302 (2006).
[38] H. Chaté, F. Ginelli, G. Grégoire, and F. Raynaud, Collective motion of self-propelled particles interacting without cohesion, Phys. Rev. E **77**, 046113 (2008).
[39] P. Romanczuk, I. D. Couzin, and L. Schimansky-Geier, Collective Motion due to Individual Escape and Pursuit Response, Phys. Rev. Lett. **102**, 010602 (2009).
[40] T. Ohta and T. Ohkuma, Deformable Self-Propelled Particles, Phys. Rev. Lett. **102**, 154101 (2009).
[41] A. M. Menzel and T. Ohta, Soft deformable self-propelled particles, Europhys. Lett. **99**, 58001 (2012).
[42] Y. Fily and M. C. Marchetti, Athermal Phase Separation of Self-Propelled Particles with No Alignment, Phys. Rev. Lett. **108**, 235702 (2012).
[43] G. S. Redner, M. F. Hagan, and A. Baskaran, Structure and Dynamics of a Phase-Separating Active Colloidal Fluid, Phys. Rev. Lett. **110**, 055701 (2013).
[44] R. Grossmann, L. Schimansky-Geier, and P. Romanczuk, Self-propelled particles with selective attraction-repulsion interaction: From microscopic dynamics to coarse-grained theories, New J. Phys. **15**, 085014 (2013).
[45] R. Grossmann, P. Romanczuk, M. Bär, and L. Schimansky-Geier, Vortex Arrays and Mesoscale Turbulence of Self-Propelled Particles, Phys. Rev. Lett. **113**, 258104 (2014); Pattern formation in active particle systems due to competing alignment interactions, Eur. Phys. J. Special Topics **224**, 1325 (2015).
[46] K. H. Nagai, Y. Sumino, R. Montagne, I. S. Aranson, and H. Chaté, Collective Motion of Self-Propelled Particles with Memory, Phys. Rev. Lett. **114**, 168001 (2015).
[47] L. Barberis and F. Peruani, Large-Scale Patterns in a Minimal Cognitive Flocking Model: Incidental Leaders, Nematic Patterns, and Aggregates, Phys. Rev. Lett. **117**, 248001 (2016); F. Peruani, Hydrodynamic equations for flocking models without velocity alignment, J. Phys. Soc. Jpn. **86**, 101010 (2017).
[48] S. Tanida, K. Furuta, K. Nishikawa, T. Hiraiwa, H. Kojima, K. Oiwa, and M. Sano, Gliding filament system giving both orientational order and clusters in collective motion, Phys. Rev. E **101**, 032607 (2020).
[49] T. Hiraiwa, A. Nagamatsu, N. Akuzawa, M. Nishikawa, and T. Shibata, Relevance of intracellular polarity to accuracy of eukaryotic chemotaxis, Phys. Biol. **11**, 056002 (2014).
[50] T. Ohta, M. Tarama, and M. Sano, Simple model of cell crawling, Physica (Amsterdam) **318D–319D**, 3 (2016).
[51] See Supplemental Material at http://link.aps.org/supplemental/10.1103/PhysRevLett.125.268104 for details of the model, extended results, discussions about comparison with Dicty's DSO, and movies and additional snapshots of numerical results, which includes Refs. [52,53].
[52] Y. Arai, T. Shibata, S. Matsuoka, M. J. Sato, T. Yanagida, and M. Ueda, Self-organization of the phosphatidylinositol lipids signaling system for random cell migration, Proc. Natl. Acad. Sci. U.S.A. **107**, 12399 (2010).
[53] T. Pérez, Y. Liu, W. Li, J. D. Gunton, and A. Chakrabarti, Pathways of cluster growth and kinetic slowing down in a model of short-range attractive colloids, Langmuir **27**, 11401 (2011).
[54] D. Grossman, I. S. Aranson, and E. B. Jacob, Emergence of agent swarm migration and vortex formation through inelastic collisions, New J. Phys. **10**, 023036 (2008).
[55] T. Hanke, C. A. Weber, and E. Frey, Understanding collective dynamics of soft active colloids by binary scattering, Phys. Rev. E **88**, 052309 (2013).
[56] E. Bertin, M. Droz, and G. Grégoire, Boltzmann and hydrodynamic description for self-propelled particles, Phys. Rev. E **74**, 022101 (2006).

[57] A. Solon, H. Chaté, and J. Tailleur, From Phase to Microphase Separation in Flocking Models: The Essential Role of Nonequilibrium Fluctuations, Phys. Rev. Lett. **114**, 068101 (2015).

[58] T. Hiraiwa, M. Y. Matsuo, T. Ohkuma, T. Ohta, and M. Sano, Dynamics of a deformable self-propelled domain, Eurphys. Lett. **91**, 20001 (2010).

[59] M. Tarama and T. Ohta, Spinning motion of a deformable self-propelled particle in two dimensions, J. Phys. Condens. Matter **24**, 464129 (2012).

[60] S. Weitz, A. Deutsch, and F. Peruani, Self-propelled rods exhibit a phase-separated state characterized by the presence of active stresses and the ejection of polar clusters, Phys. Rev. E **92**, 012322 (2015).